‘‘Multifunctional Ni-Mn-Ga and Ni-Mn-Cu-Ga Heusler particles towards the nanoscale by ball-milling technique’’

"Multifunctional Ni-Mn-Ga and Ni-Mn-Cu-Ga Heusler particles towards the nanoscale by ball-milling technique''

Greta Cavazzini, Francesco Cugini, Davide Delmonte, Giovanna Trevisi, Lucia Nasi, Semih Ener, David Koch, Lara Righi, Massimo Solzi, Oliver Gutfleisch, Franca Albertini

PII: S0925-8388(21)01156-7

DOI: https://doi.org/10.1016/j.jallcom.2021.159747

Reference: JALCOM159747

To appear in: *Journal of Alloys and Compounds*

Received date: 7 January 2021
Revised date: 6 March 2021
Accepted date: 27 March 2021

Please cite this article as: Greta Cavazzini, Francesco Cugini, Davide Delmonte, Giovanna Trevisi, Lucia Nasi, Semih Ener, David Koch, Lara Righi, Massimo Solzi, Oliver Gutfleisch and Franca Albertini, "Multifunctional Ni-Mn-Ga and Ni-Mn-Cu-Ga Heusler particles towards the nanoscale by ball-milling technique'', *Journal of Alloys and Compounds,* (2021) doi:https://doi.org/10.1016/j.jallcom.2021.159747

''Multifunctional Ni-Mn-Ga and Ni-Mn-Cu-Ga Heusler particles towards the nanoscale by ball-milling technique''

Greta Cavazzini [a,b,*], Francesco Cugini [a,b], Davide Delmonte [a], Giovanna Trevisi [a], Lucia Nasi [a], Semih Ener [c], David Koch [c], Lara Righi [d], Massimo Solzi [b], Oliver Gutfleisch [c], and Franca Albertini [a]

[a] *Institute of Materials for Electronics and Magnetism – Consiglio Nazionale delle Ricerche, Parco Area delle Scienze 37/A, 43124 Parma, Italy*

[b] *Department of Mathematical, Physical and Computer Sciences, University of Parma, Parco Area delle Scienze 7/A, 43124 Parma, Italy*

[c] *Institute of Material Science, Technical University of Darmstadt, Alarich-Weiss-Str. 16, 64287 Darmstadt, Germany*

[d] *Department of Chemistry, Life Sciences and Environmental Sustainability, University of Parma, Parco Area delle Scienze 17/A, 43124 Parma, Italy*

[*] Corresponding author:

Email address: greta.cavazzini@studenti.unipr.it

Postal address: Parco Area delle Scienze 37/A, 43124 Parma, Italy

Abstract

This work presents a top-down method, based on ball-milling techniques, for the preparation of $Ni_{50}Mn_{30}Ga_{20}$ and $Ni_{50}Mn_{18.5}Cu_{6.5}Ga_{25}$ micro-meter and sub-micro-meter sized particles. The structural, morphological, and magnetic features of the as-milled and annealed particles are investigated. First, we observe a detrimental effect on the magnetic properties and magneto-structural phase transitions of the induced lattice defects and atomic disorder, and second, we demonstrate the possibility to recover the original configuration by subsequent annealing. The optimization of the latter is strongly dependent on the initial milling energy, but, generally, a fast recovery of the Heusler and martensitic phases is observed. Further, we can tune the transformation temperatures or

even improve the magnetic properties, in terms of phase homogeneity, thermal hysteresis and saturation magnetization, by decreasing the particles' size of the examined compounds.

Keywords: Heusler alloys; Martensitic transformation; Mechanical milling; Magnetic properties; Magnetic nanoparticles.

1. Introduction

Ferromagnetic Ni-Mn-Ga Heusler compounds, belonging to the large class of multifunctional Ni-Mn-X compounds (with X= Ga, In, Sn, …), have been extensively investigated in the bulk form. This strong interest is related to the particular coupling of ferromagnetic, ferro-elastic and thermal properties, enabled by a thermo-elastic martensitic transformation, and to the extraordinary tunability of the transition temperatures with composition [1,2]. Giant magnetic shape memory and magneto-caloric effects have made Ni-Mn-X Heusler benchmark materials for potential application in sensing and actuation devices [3], and for the solid-state magnetic refrigeration technology [4]. Regarding the latter application, a large and reversible magnetocaloric effect, near room-temperature, is the key-prerequisite for the development of magnetic cooling devices, as a low-carbon and more efficient alternative to the conventional gas-compression methodology [5–7].

The phase diagrams reported for Ni-Mn-Ga Heusler compounds [1,2] show the onset of specific magneto-structural behaviours by increasing Ni and/or Mn excess over Mn and/or Ga atoms, respectively. For specific concentration ranges, the overlap between the structural martensitic transformation and the magnetic Curie transition of the austenite gives rise to a coupled magneto-structural transformation, from a low

temperature, low symmetry, ferromagnetic martensite, to a high temperature, high symmetry, paramagnetic austenite, as for $Ni_{50}Mn_{30}Ga_{20}$ compound. Even though the associated magnetocaloric effect is significant [8,9], it is not useful for the magnetic refrigeration around room temperature, due to the high temperature of the coupled transformation (as for instance $T_C \approx$360 K, Ref. [1]) and its limited reversibility.

Nevertheless, it has been reported [10–13] the possibility to simultaneously reduce the Curie temperature and maintain the coupling with the martensitic transformation by substituting Mn by Cu, in quaternary $Ni_{50}Mn_{25-x}Cu_xGa_{25}$ Heusler alloys, with x= 5.5, 6, 6.5. The coupling of the magnetic and structural transformation near room temperature is interesting also for the development of novel biomedical applications [14].

Hence, these compounds could offer great potential from the technological point of view, since they are based on non-critical elements and can be widely employed in many fields of application. It follows that a fundamental prerequisite is the preservation of the magneto-structural coupling and related functional properties by changing the sample morphology for the specific purpose, as in form of magnetic nanoparticles for the magnetic-hyperthermia cancer therapy [15].

Several new morphologies of the Ni-Mn-Ga compound, as foam-like structures [16,17], thin films [18,19], nano-disks [20], ribbons [21,22] or smart composites [23], have been largely investigated in the last decade, also because they show interesting advantages for technological applications over the bulk, such as higher mechanical stability and ductility, faster heat-exchange and lower eddy-current losses.

However, a strong influence of sample dimensions and grain-size on the peculiar martensitic characteristics has been revealed [22,24,25]. Therefore, a lot of work is still required to assess the preparation of Heusler nanoparticles able to show the martensitic phase transformation as in the bulk.

Ball-milling is a cost-effective and versatile top-down method to decrease the particle size and is well-established on an industrial scale for the preparation of micro- and sub-micro-meter sized materials of different nature. This technique needs careful balancing several milling parameters, for instance, the ball-to-powder weight ratio, the ball-milling speed or frequency, the milling atmosphere and milling time, which together determine the efficiency of grinding and the final morphology of the particles [26–28].

Few works by Tian *et al*. [29–31] and Wang *et al*. [32] have reported about the fabrication of micro-meter or nano-meter sized particles of Ni-Mn-Ga by using high-energy ball-milling methods. They have shown that the structural and magnetic phase transitions of the post-milled annealed particles are determined by their size and degree of atomic order. By contrast, the cryo-milling technique, or ball-milling at cryogenic temperature, has not been tested to reduce particle and/or grain size for this kind of intermetallic alloys. This method might be advantageous, since it can increase the fracture rate of otherwise cold-welded particles, and, hence, reduce more rapidly the particle size [28,33].

Our work focuses on the preparation and characterization of micron and submicron $Ni_{50}Mn_{30}Ga_{20}$ and $Ni_{50}Mn_{18.5}Cu_{6.5}Ga_{25}$ Heusler particles by means of a variety of ball-milling techniques. The two compositions were selected in order to achieve the overlap between magnetic and structural transformations. Copper was added to shift the coupled transition around room-temperature, thus making the compound interesting for technological applications, such as the magnetic refrigeration at room-temperature or the magnetic hyperthermia for biomedical applications.

The starting bulk materials have been subjected to high-energy ball-milling, cryo-milling and wet planetary ball-milling, with addition of a solvent as well as surfactants. The particles' morphology, structure and magneto-thermal properties after the different

mechanical deformation processes have been analysed and assessed in terms of the effectiveness of the ball-mill method to reduce the particle's size while preserving the composition. In the attempt to obtain multifunctional micro- and sub-microparticles, different annealing conditions have been tested and varied to optimize the recovery of the original phase transitions.

The work demonstrates the feasible preparation of micro and sub-microparticles of Ni-Mn-Ga and Ni-Mn-Cu-Ga compounds by carefully tuning the milling parameters and highlights the differences and/or improvements in the magneto-structural properties of the powders as compared to the bulk.

2. Materials and methods

2.1. Bulk synthesis

Two bulk polycrystalline ingots, with nominal composition $Ni_{50}Mn_{30}Ga_{20}$ and $Ni_{50}Mn_{18.5}Cu_{6.5}Ga_{25}$ (at. %), were prepared by arc-melting technique, under argon atmosphere, using high purity elements (99.9%), with an addition of 1.5 wt.% Mn, to compensate for evaporation losses during the melting process. The ingots were melted four times, turning them upside down each time, and were homogenized in a quartz tube, filled with argon, at 850°C, for 3 days, followed by water quenching.

2.2. Ball-milling processes

The bulk pieces were hand-grinded (HG) in an agate mortar to prepare powder of particle size less than 160 μm, which was used as the starting material for the subsequent ball-milling processes.

2.2.1. Cryo-milling

HG powder of Ni-Mn-Ga and Ni-Mn-Cu-Ga was subjected to the cryo-milling process, using a Retsch Shaker Cryo-mill (CM). It was selected a frequency of 15 Hz, a

single stainless-steel ball of 20 mm diameter, and a ball-to-powder weight ratio of 12:1. The HG powder was sealed in the jar under protective Ar atmosphere. Then, the milling process was conducted under constant external flow of liquid nitrogen, in intervals of 5 min milling and 2.5 min rest, to avoid overheating during the milling process, up to a maximum effective milling time of 2 and 3 h, for Ni-Mn-Ga and Ni-Mn-Cu-Ga compounds, respectively.

2.2.2. High-energy vibration ball-milling

Ni-Mn-Ga HG powder was subjected to the high-energy vibration ball-milling (HEBM) using a SPEX-8000 mill, with a jar and 4 balls, of 12 mm diameter, made of stainless steel and a ball-to-powder weight ratio 10:1, under a protective Ar atmosphere. The process was run in 30 min milling and 1 h rest, up to a total milling time of 8 h.

2.2.3. Wet Planetary ball-milling

On the basis of the results obtained for Ni-Mn-Ga (see below), and for the possibility to use a solvent and a surfactant in the jar, for the second batch of Ni-Mn-Cu-Ga HG powder, it was tested the planetary ball-milling (PBM) instead of the HEBM.

The Fritsch planetary ball-mill Pulverisette 7 was employed, selecting a rotational speed of 300 rpm, a ball-to-powder ratio of 10:1, and using Zirconia media, with spheres of 5 mm diameter. Isopropanol was added as a liquid milling medium to reduce overheating and enhance particles' dispersion. The process was conducted in intervals of 10 min milling and 5 min rest, up to 35 h of milling.

2.2.4. Cryo-milling + Surfactant-Assisted Planetary ball-milling

Moreover, it was tested a two-steps process, consisting in the combination of cryo-milling (till 3 h) and surfactant-assisted planetary ball-milling (SAPBM), using oleic

acid (20 wt. %) as surfactant, and n-heptane, as solvent, for several hours of milling (14 h), aimed at investigating and comparing the effects on particle size reduction and distribution with respect to the wet PBM particles.

2.3. Annealing treatments

The obtained powders were subjected to several annealing treatments, by varying temperature, time, and cooling rate, in order to eliminate the mechanically induced defects and stresses and investigate the effect of thermal energy on the phase transformations.

Wrapped in small packets of Ta, the powders were annealed in a resistance furnace under Ar atmosphere and slowly cooled or water quenched, afterwards.

For the HG powder of both compounds, the thermal treatments were performed at a fixed time of 4 h and at the two temperatures 500°C and 600/630°C, followed by slow cooling or water quenching, as reported in **Tables 1** and **2**, for Ni-Mn-Ga and Ni-Mn-Cu-Ga, respectively.

For Ni-Mn-Ga CM and HEBM particles, it was fixed an annealing duration of 1 h and it was varied the annealing temperature from 300°C up to 1000°C, followed by water quenching. The annealing treatments for the CM particles were optimized by increasing the annealing time to 4 h and reducing the cooling rate (slow cooling), as reported in **Table 1**.

Similarly, the Ni-Mn-Cu-Ga CM particles were subjected to an annealing treatment for 4 h at 630°C, followed by slow cooling; instead, the long-milled wet PBM and CM+SAPBM ones were annealed at a higher temperature (755°C) and/or for a longer time (24 h), as specified in **Table 2**.

Sample: $Ni_{49.4}Mn_{30.3}Ga_{20.3}$	Milling time (h)	Annealing temperature (°C)	Annealing time (h)	Cooling rate	Corresponding Name
Hand-grinded (HG)	-	-	-	-	HG
		500-600	4	SC	HG4h500SC
				WQ	HG4h600WQ
Cryo-milled (CM)	1	-	-	-	CM-1h
	2	-	-	-	CM-2h
		300-400-	1	WQ	2CM300WQ 2CM400WQ
		500-630-	1 4	WQ	SC WQ	2CM500WQ 2CM630WQ	2CM4h500SC 2CM4h630WQ
		750-1000	1	WQ	2CM750WQ 2CM1000WQ
High-energy ball milled (HEBM)	1	-	-	-	HEBM-1h
	2	-	-	-	HEBM-2h
	8	-	-	-	HEBM-8h
		300-400-500-790-1000	1	WQ	8HEBM300WQ 8HEBM400WQ 8HEBM500WQ 8HEBM790WQ 8HEBM1000WQ

Table 1: Milling procedure, milling time, and annealing treatment specifications of the as-prepared and post-annealed $Ni_{49.4}Mn_{30.3}Ga_{20.3}$ powder samples.

Sample: $Ni_{49.7}Mn_{18.7}Cu_{6.4}Ga_{25.2}$	Milling time (h)	Annealing temperature (°C)	Annealing time (h)	Cooling rate	Corresponding Name
Hand-grinded (HG)	-	-	-	-	HG
		500	4	WQ	HG4h500WQ
		630			HG4h630WQ
Cryo-milled (CM)	2	500	4	WQ	2CM4h500WQ
		630		SC	2CM4h630SC
	3	-	-	-	CM-3h
		630	4	WQ	3CM4h630WQ
Planetary Ball-milled with isopropanol (wet PBM)	19	-	-	-	wetPBM-19h
		755	24	SC	19PBM1d755SC
	35	755	24	SC	35PBM1d755SC
Cryo-milled (CM) + Planetary Ball-milled with surfactant-assistance (SAPBM)	3 + 8	-	-	-	SAPBM-8h
	14	755	24	SC	SAPBM4h755SC

Table 2: Milling procedure, milling time, and annealing treatment specifications of the as-prepared and post-annealed $Ni_{49.7}Mn_{18.7}Cu_{6.4}Ga_{25.2}$ powder samples.

2.4. Characterization

The morphology, microstructure, and chemical composition of the starting ingots and prepared powders were analysed by a Scanning electron microscope SEM-FIB

Zeiss Auriga Compact, equipped with an INCA Energy Dispersive X-ray (EDX) Spectroscopy system.

Using the ImageJ software, the SEM images were processed to calculate the particles' sizes. The resulting values of particle size were collected in a histogram with the following binned size for the different powders analysed: 10 μm for the Ni-Mn-Ga CM-2h and HEBM-2h powders and the Ni-Mn-Cu-Ga CM-3h powder; 5 μm for the Ni-Mn-Cu-Ga wetPBM-19h; 0.5 μm for the Ni-Mn-Cu-Ga SAPBM-8h one.
The histograms were fitted with a Gaussian or Lorentzian curve to determine the average particle size and distribution.

The structural analysis at room temperature was carried out by powder X-ray diffraction (XRD) measurements using a STOE STADI P in transmission geometry with Mo Kα_1 radiation. For temperature-dependent X-ray measurements, it was used a custom-built setup in transmission geometry with Mo Kα radiation and Mythen2 R 1K Detector (Dectris Ltd.). The sample was mixed with NIST 640d standard silicon powder for correcting geometric errors and glued on a graphite foil. The temperature was controlled by means of a closed cycle He-cryo-furnace.
The X-ray diffractograms were analysed by the Le Bail refinement, with Jana2006 software [34].

Low-field ac magnetic susceptibility measurements were carried out as a function of temperature in a home-built device to determine the magnetic and/or the coupled magneto-structural transitions.

Temperature-dependent magnetization measurements (M(T)) were performed under 10 mT and 1 T external magnetic field, following the field-cooling (FC) and field-cooled-warming (FCW) procedures, in a SQUID magnetometer (MPMS-XL5 by Quantum Design) and in an extraction magnetometer (MAGLAB SYSTEM2000 by Oxford Instruments).

3. Results

3.1. Bulk materials

The magnetic and magneto-structural phase transitions of $Ni_{49.4\pm0.4}Mn_{30.3\pm0.6}Ga_{20.3\pm0.4}$ and $Ni_{49.7\pm0.4}Mn_{18.7\pm0.2}Cu_{6.4\pm0.1}Ga_{25.2\pm0.3}$ samples are displayed in **Figs**. **1(a)-(b)**, respectively.

In **Fig. 1(a)**, for $Ni_{49.4}Mn_{30.3}Ga_{20.3}$, it can be noted the occurrence of the magneto-structural martensitic transformation, in proximity of 365 K, as indicated by the increase of the magnetic susceptibility, from the low-temperature martensitic phase, with a high magneto-crystalline anisotropy [35], to the high temperature, ferromagnetic cubic austenite, which immediately transforms to the paramagnetic state (Curie transition).

At the Curie transition, the magnetic susceptibility presents two different inflections, denoted with $T_{C,1}^{A}$ and $T_{C,2}^{A}$, where on the second one, at 375 K, it is found a small thermal hysteresis between the heating and cooling branches. This is the indication of the overlap with the structural martensitic transformation. Instead, at temperature lower than $T_{C,1}^{A}$, it is visible a much larger hysteresis opening between the forward and reverse martensitic transformation temperatures, labelled with $T_{fwd,1}$ and $T_{rev,1}$. This fact highlights that the structural and magnetic transitions are close to each other but not uniformly coincident in the sample.

By contrast, in **Fig. 1(b)**, the ac magnetic susceptibility of $Ni_{49.7}Mn_{18.7}Cu_{6.4}Ga_{25.2}$ sample shows a single, hysteretic, coupled magneto-structural transition, from a ferromagnetic martensite, at low temperature, to a paramagnetic austenite at high temperature, in the temperature interval 310-325 K. Hence, both in heating and in cooling branches, the martensitic transformation is coincident with the Curie transition temperature of the austenite, leading to a large and sharp change of the magnetic signal, accompanied by a thermal hysteresis of approximately 10 K.

The results of both systems are in good agreement with the expected behaviours for $Ni_{50}Mn_{30}Ga_{20}$ [1] and $Ni_{50}Mn_{18.5}Cu_{6.5}Ga_{25}$ [13] bulk Heusler compounds.

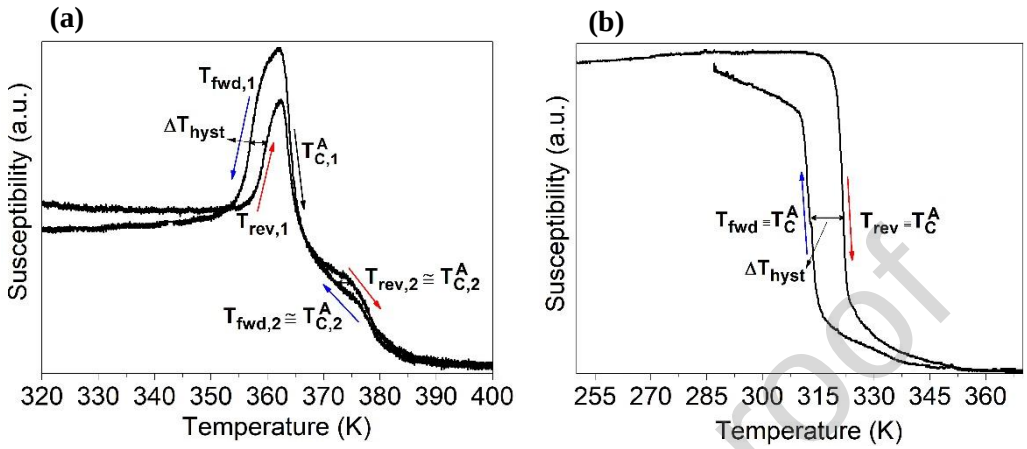

Figure 1: Magnetic susceptibility measurement as a function of temperature for the bulk sample of **(a)** $Ni_{49.4}Mn_{30.3}Ga_{20.3}$ and **(b)** $Ni_{49.7}Mn_{18.7}Cu_{6.4}Ga_{25.2}$, with indication of the transformation temperatures in heating and cooling branches.

3.2. Ball-milled Ni-Mn-Ga powders

Figs. 2 (a)-(b) show the SEM micrographs and the corresponding size distributions (in the inset) of $Ni_{49.4}Mn_{30.3}Ga_{20.3}$ powders after 2 h of cryo-milling (CM-2h) and high-energy ball-milling (HEBM-2h, **Table 1**).

During the CM process (**Fig. 2(a)**), the particles tend to elongate and get thinner, reaching a thickness of ~5 µm and a length of bimodal size distribution, with two peaks at around 30±10 and 75±15 µm, as revealed in the inset.

In contrast, during the HEBM process (**Fig. 2(b)**), the starting material (HG powder) breaks into chunk particles of ~15-20 µm thickness, with a homogeneous Gaussian size distribution peaked at 46±13 µm, as shown in the inset. However, even after 8 h of HEBM, the particles present a length of 30±10 µm and thickness of 15±5 µm (not shown here).

By the EDX analysis, instead, it has been confirmed the overall preservation of the bulk chemical composition, such as $Ni_{49.5\pm0.2}Mn_{30.2\pm0.1}Ga_{20.3\pm0.2}$ for the CM-2h particles and $Ni_{48.4\pm0.6}Mn_{31.2\pm1}Ga_{20.4\pm0.6}$ for the HEBM-8h particles.

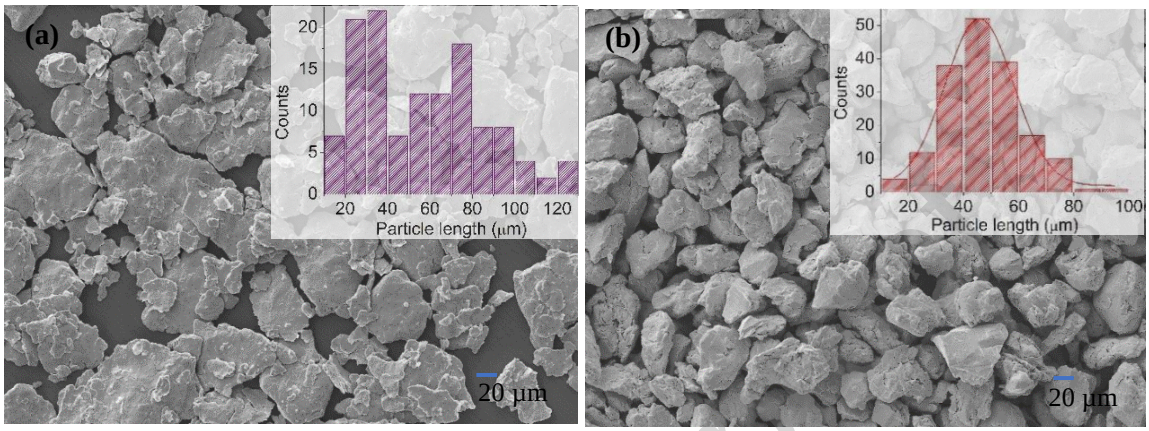

Figure 2: SEM images of $Ni_{49.4}Mn_{30.3}Ga_{20.3}$ powders after 2 h of **(a)** CM and **(b)** HEBM process. Insets: corresponding particle size distribution.

The XRD patterns of **Figs. 3(a)-(b)** show that a different structural evolution takes place between the CM and HEBM powders as a function of the milling time.

At room-temperature, the starting HG powder presents a tetragonal structure, referred to the non-modulated (NM) martensitic phase (bottom pattern of **Figs. 3**, lattice parameters in **Table 3**). After 1 h of CM process, the original structure disorders, as highlighted by the peak broadening (CM-1h, **Fig. 3(a)**), while, after the HEBM, it transforms into a disordered cubic phase (HEBM-1h, **Fig. 3(b)**), as denoted by the suppression of the tetragonal peaks and the appearance of new ones in different positions.

On increasing the milling duration, the peak broadening increases for the CM-2h powders, leading to the almost suppression of the tetragonal phase and, besides, it is possible to notice the same reflections of the HEBM powders, referred to as a disordered fcc structure. In the HEBM-2h and HEBM-8h diffractograms, instead, it emerges an asymmetric broadening of the fundamental cubic peak at 2θ=19.3°, which is not present in that of the CM-2h powder. As highlighted by the Le Bail refinement, this

is due to the presence of a secondary cubic phase, indexed as ''A fcc'', since it shows the same lattice constant a=5.85 Å of the cubic austenitic phase of the HG powder, which becomes stable at temperature above 365 K (XRD pattern not shown here; see **Table 3** for lattice parameters).

The structural transformation from the bct structure to the higher symmetric fcc phase, during ball-milling, has been observed and reported also by Wang *et al*. [32] and Tian *et al*. [30,31] for Ni-Mn-Ga particles prepared by the high-energy ball milling process, in dry conditions. Whereas it has not been detected, by the same authors, after the use of the planetary ball-milling technique with a liquid milling medium.

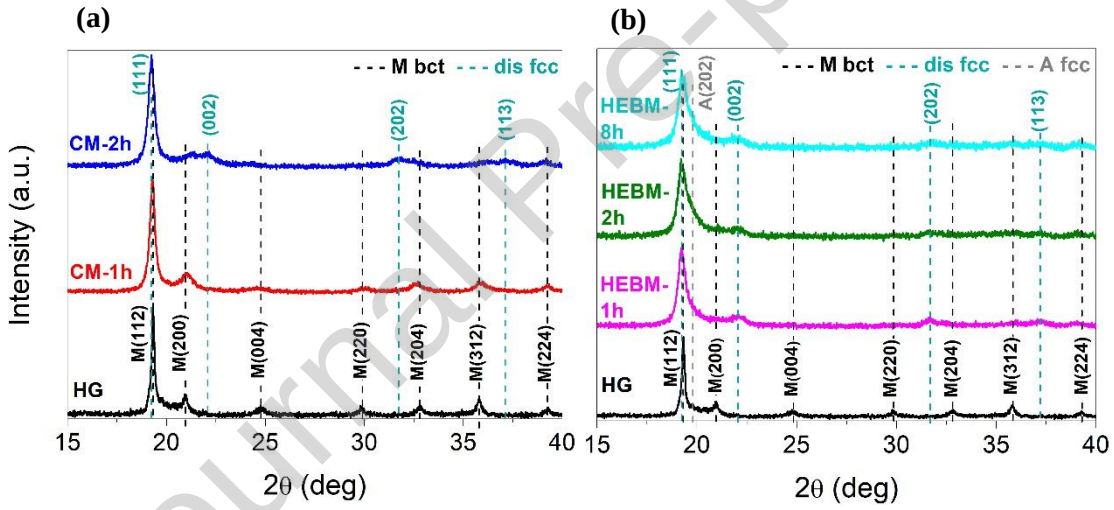

Figure 3: Room-temperature XRD patterns of $Ni_{49.4}Mn_{30.3}Ga_{20.3}$ powders after **(a)** CM process for 1h-2h, and **(b)** HEBM process for 1h-2h-8h, in comparison to the diffraction pattern of the HG powder.

Powder	Crystal phases	Cell parameters			
HG: @ RT:	**Martensite NM** bct	**a**=3.8961 ±0.0007 Å	**b**=3.8961 ±0.0007 Å	**c**=6.584 ±0.002 Å	$\alpha = \beta = \gamma$= 90°
@ 400 K:	**Austenite** fcc $(L2_1)$	**a**=5.849 ± 0.007 Å	**b**=5.849 ± 0.007 Å	**c**=5.849 ± 0.007 Å	$\alpha = \beta = \gamma$= 90°
HG4h600WQ @ RT:	**Martensite** $7M$ **modulated**	**a**=4.2325 ±0.0005 Å	**b**=5.5215 ±0.0005 Å	**c**=4.2751 ±0.0005 Å	$\alpha = \gamma$=90° β=93.35 ±0.01 °
	Modulation Vector	q (Å^{-1})= 0.2947 ±0.0009 a^*			

Table 3: Characteristic crystallographic data of the hand-grinded (HG) and post-annealed (HG4h600WQ) $Ni_{49.4}Mn_{30.3}Ga_{20.3}$ powders, obtained by the Le Bail refinement of the XRD patterns.

The comparison between the thermomagnetic responses of bulk, HG powder, CM-2h and HEBM-8h powders is presented in **Fig. 4**. The HG powder shows the almost suppression of the first reverse martensitic transformation, detected at $T_{rev,1}$ in the bulk, and the increase of phase fraction transforming with a coupled magneto-structural transformation at a higher temperature, coincident with the $T_{rev,2} \equiv T_{C,2}^{A}$ of the bulk. Instead, the CM-2h and HEBM-8h powders show a complete suppression of both the ferromagnetism and the magneto-structural transformation.

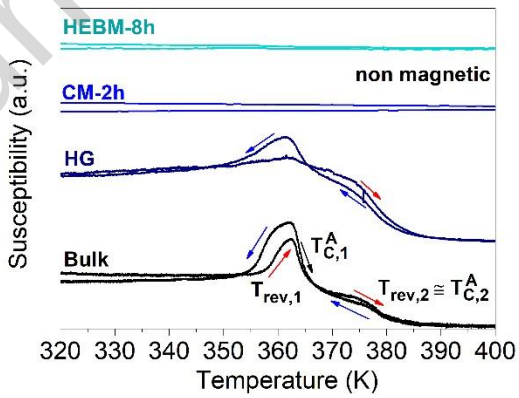

Figure 4: Low-field thermomagnetic responses of bulk, HG powder, CM-2h and HEBM-8h powders of $Ni_{49.4}Mn_{30.3}Ga_{20.3}$ compound.

Overall, the analysis on Ni-Mn-Ga ball-milled powders shows that with the lower energetic cryo-milling process, it is possible to obtain in 2 h flaky particles of 20 μm length and 2-5 μm thickness. They are thinner and preserve a higher crystallinity, as

compared to the chunky powders of 30 μm length and 10 μm thickness achieved after the high-energy vibration ball-milling for a longer milling time (i.e., 8 h).

3.3. Ball-milled Ni-Mn-Cu-Ga powders

Figure 5(a)-(b) shows the morphology of the $Ni_{49.7}Mn_{18.7}Cu_{6.4}Ga_{25.2}$ ball-milled powders prepared by CM for 3 h and PBM with isopropanol for 19 h.

In both cases, the compound is deformed into elongated and thin particles similar to flakes. The CM-3h particles present an average thickness of ~5 μm and a Gaussian length distribution well peaked at around 37±18 μm (**Fig. 5(a)**). The wetPBM-19h ones, instead, are significantly smaller and thinner, showing a Lorentzian size distribution peaked at 8±6 μm length and a rapid decrease of concentration for particles bigger than 20 μm (**Fig. 5(b)**). Moreover, sub-micron meter sized particles of 800-900 nm have been achieved in this powder batch.

A much more effective particle size reduction down to the sub-micrometre scale has been obtained by using the surfactant (oleic acid) during the PBM process, after the CM one, as visible in the SEM micrographs of **Fig. 5(c)**. These are referred to the SAPBM-8h particles (**Table 2**) and point out the formation of a large amount of submicron particles, having the thickness of 100-150 nm and the length in the range of 250-750 nm.

The composition of the ball-milled particles was assessed by EDX analysis ($Ni_{49.4\pm0.6}Mn_{19\pm0.3}Cu_{6.5\pm0.2}Ga_{25.1\pm0.3}$) and resulted to be consistent with the original one.

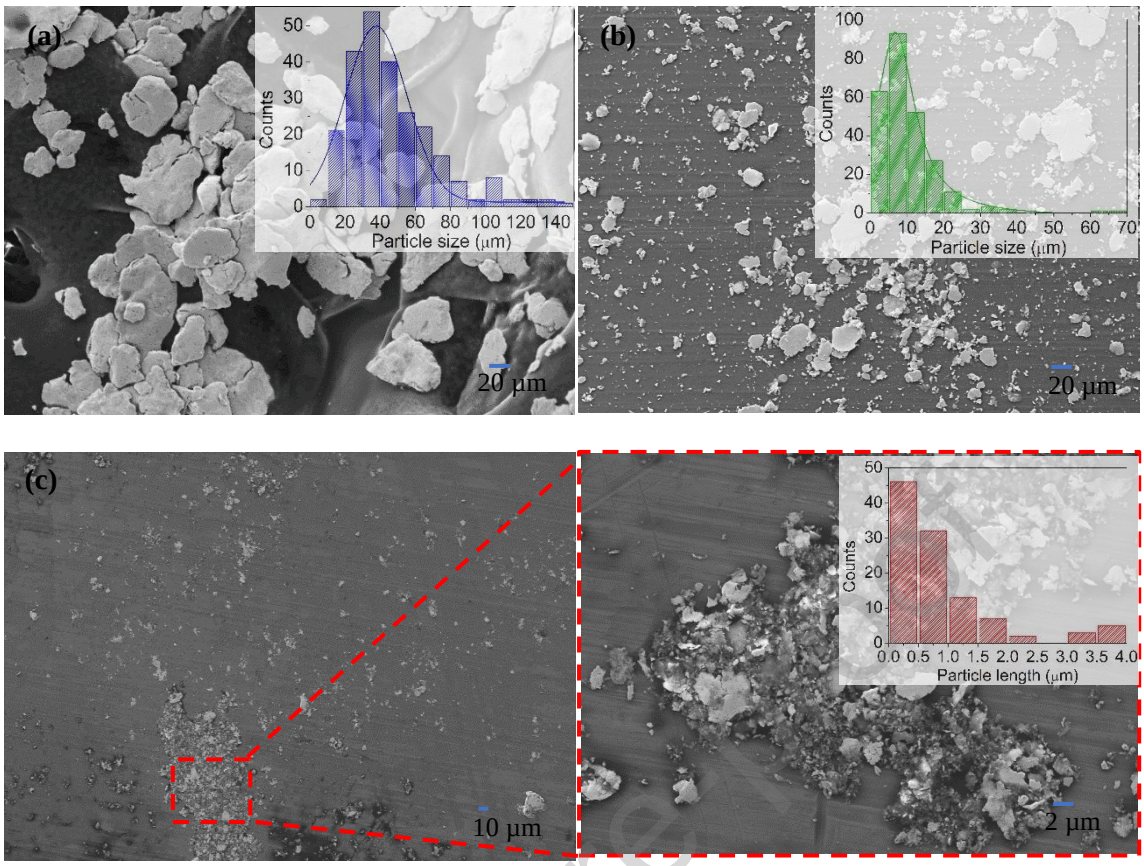

Figure 5: SEM micrographs of the $Ni_{49.7}Mn_{18.7}Cu_{6.4}Ga_{25.2}$ particles after **(a)** 3 h of CM process, **(b)** 19 h of wet PBM process, **(c)** and 8 h of SAPBM process, following the CM one. Insets: corresponding particle size distributions.

The room-temperature XRD measurements of the CM-3h and wetPBM-19h powders are shown in **Fig. 6(a)**, where at the bottom is reported the initial crystal structure of the HG particles, characterized by a mixture of NM tetragonal martensite and cubic austenite (**Table 4**). Both types of ball-milled powders display a deformed disordered *bct* phase, as pointed out by the broadening of the peaks and the non-uniform shift of the fundamental reflections of the martensite. This effect is compatible with an anisotropic lattice strain of the original tetragonal unit cell during the ball-milling process, and, possibly, it can be related to the oblate shape of the particles seen in **Fig. 5**. Surprisingly, any significant difference in peak intensity, position, and/or broadening is detected between the two samples, even though the milling methods and milling parameters employed are consistently different.

With respect to the Ni-Mn-Ga ball-milled particles, it is noted that the original *bct* martensitic structure, even if it undergoes a process of disordering due to the grain-size refinement and the mechanical-induced defects, does not transform to the higher symmetric cubic structure, but rather remains stable against longer mechanical milling processes.

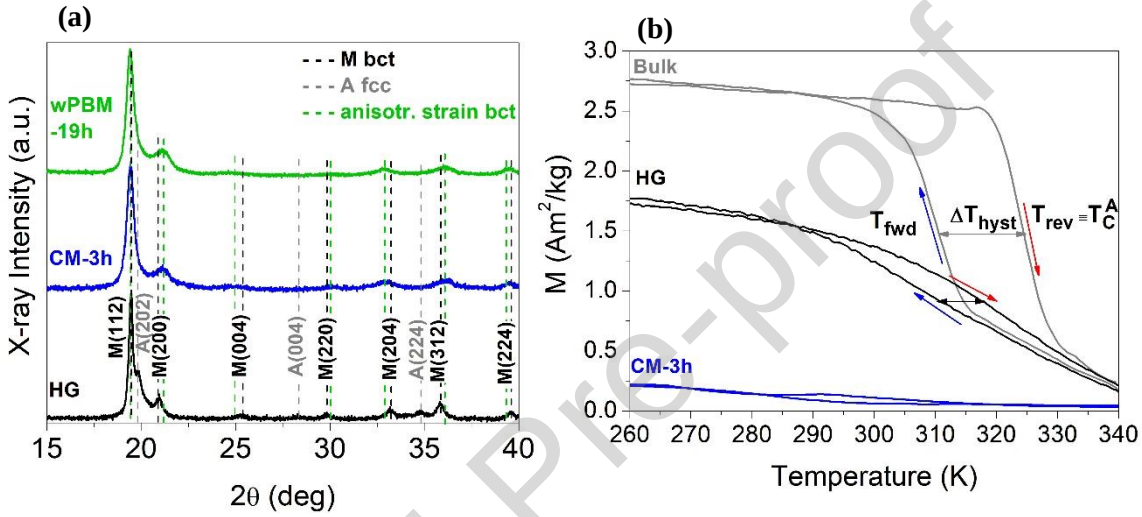

Figure 6: **(a)** Room-temperature XRD patterns of $Ni_{49.7}Mn_{18.7}Cu_{6.4}Ga_{25.2}$ powders HG, CM for 3 h and wet PBM for 19 h. **(b)** Low-field (10 mT) thermo-magnetization measurements of bulk, HG and CM-3h powders.

Powder	Crystal phases	Cell parameters			
HG: @ RT	**Martensite NM *bct* ($L1_0$)**	**a**=3.901 ±0.001 Å	**b**=3.901 ±0.001 Å	**c**=6.454 ±0.002 Å	$\alpha = \beta = \gamma$= 90°
	Austenite *fcc* ($L2_1$)	**a**=5.8140 ±0.0015 Å	**b**=5.8140 ±0.0015 Å	**c**=5.8140 ±0.0015 Å	$\alpha = \beta = \gamma$= 90°
HG4h630WQ: @ 350 K:	**Austenite *fcc* ($L2_1$)**	**a**=5.8120 ±0.0002 Å	**b**=5.8120 ±0.0002 Å	**c**=5.8120 ±0.0002 Å	$\alpha = \beta = \gamma$= 90°
@ 280 K:	**Martensite 7*M* modulated**	**a**=4.2406 ±0.0006 Å	**b**=5.5193 ±0.0004 Å	**c**=4.3049 ±0.0002 Å	$\alpha = \gamma = 90°$ β=93.033 ±0.008°
	Modulation vector	q (Å^{-1})= 0.2770 ±0.0005 c^*			

Table 4: Crystallographic data of the $Ni_{49.7}Mn_{18.7}Cu_{6.4}Ga_{25.2}$ hand-grinded and post-annealed planetary ball-milled powders, obtained by the Le Bail refinement of XRD measurements at RT.

As revealed in **Fig. 6(b)**, the thermomagnetic behaviour of the HG and CM particles shows notable changes as compared to the bulk, similarly to what previously observed and described for the Ni-Mn-Ga ball-milled particles. The HG powder of Ni-Mn-Cu-Ga compound presents a significant broadening of the coupled magneto-structural transformation, associated with a reduction of thermal hysteresis and magnetic moment of the martensitic phase, leading to a consequent lowering of the magnetization change across the transition. For the CM-3h powder, these features are drastically worsened and eventually a complete destruction of both magnetic and magneto-structural behaviour is obtained for longer milling procedures.

By testing different milling times for the planetary ball-milling process with only isopropanol or a mixture of heptane and oleic acid, it has emerged that by combining a first short (3 h) cryo-milling process with a second longer (8-14 h) surfactant-assisted planetary ball-milling (with oleic acid (20 wt.%) + heptane), the preparation of nanoparticles is more reliable and advantageous as compared to the use of only isopropanol. In fact, upon the same rotational speed of 300 rpm, a lower total milling time (14 h rather than 35 h) is required to obtain smaller sub-micron particles, of 100 nm thickness and 250 nm length, with respect to those of 250 nm thickness and 500 nm length, obtained by PBM with isopropanol.

3.4. Post-annealed Ni-Mn-Ga powders

After the grinding and milling processes, several annealing treatments have been performed on the Ni-Mn-Ga powders to recover the original crystal structure and the coupled magneto-structural phase transition, as summarized in **Table 1**.

The XRD diffractograms on the bottom of **Figs. 7(a)-8(a)** reveal that at room temperature the annealed HG4h600WQ powder is characterized by a seven-layered modulated martensite (7M) with a monoclinic superstructure (**Table 3**), as expected for

the stress-released particles [36], melt spun ribbons [9] and bulk sample [37] of the same composition.

The thermomagnetic measurement of such heat-treated powder, in **Figs. 7(b)-8(b)**, shows a magneto-structural behaviour improved with respect to the as-crushed powder (**Fig. 4**) and close to that of the bulk, with the difference of a temperature-range reduction of the coupled magneto-structural transformation and its shift to a slightly lower temperature.

Concerning the post-annealed CM-2h powder, the recovery of both crystallographic order and ferromagnetism takes place gradually by increasing the annealing temperature (**Fig. 7(a)-(b)**). After the annealing at 300°C, the structure of the 2CM300WQ powder is still disordered as highlighted by the presence of only two not well-defined and broad peaks. These seem to intensify for the 2CM400WQ powder. In addition, for this powder, it is possible to detect a change in the magnetic susceptibility signal associable to a slight hint of the magnetic Curie transition (**Fig. 7(b)**).

After annealing at temperature 500°C, the crystallographic reflections become more intense and defined and a broad Curie transition is recognized by the susceptibility measurement. On shortly annealing at temperature between 500-630°C, a complete atomic ordering process is reached, giving rise to the restoration of the 7M modulated martensitic phase in the XRD pattern of the 2CM630WQ powder. These annealing conditions lead to the recovery of the coupled magneto-structural transformation close to the one of HG4h600WQ powder. However, with respect to the latter, it is observed a larger broadening of the susceptibility signal below 360 K, both in heating and cooling branches. Interestingly, by further increasing the annealing temperature between 750°C and 1000°C, the thermomagnetic response undergoes an enhancement of broadening, accompanied by the shift to higher temperatures of the coupled magneto-structural transition, especially for the 2CM1000WQ. For this powder, the XRD measurement

reveals an almost suppression of the 7M modulated structure and the appearance of the characteristic peaks of the tetragonal NM martensite (**Fig. 7(a)**).

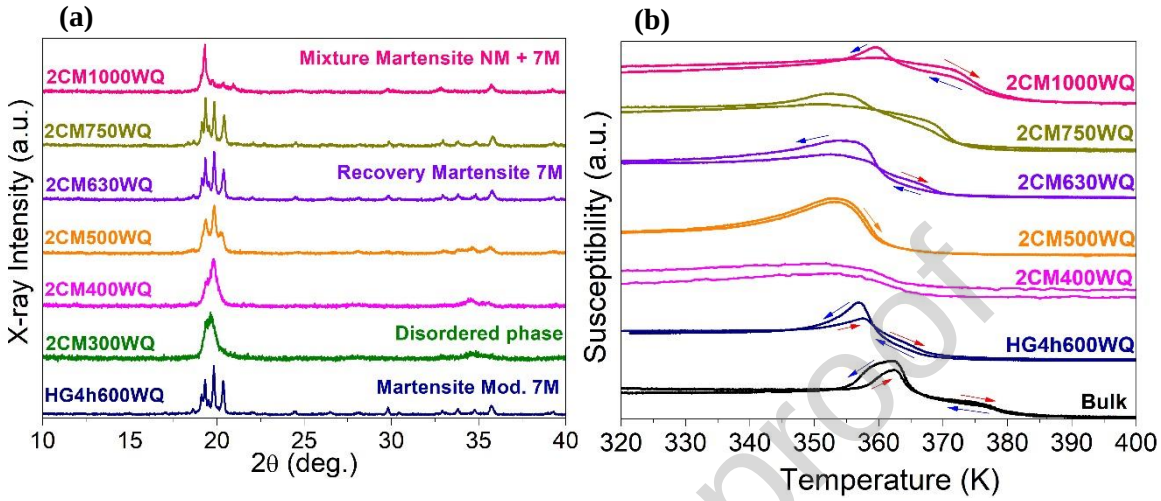

Figure 7: **(a)** Room-temperature XRD spectra of the $Ni_{49.4}Mn_{30.3}Ga_{20.3}$ post-annealed CM-2h powders as a function of the annealing temperature, in comparison to the post-annealed hand-grinded powders (HG4h600WQ). **(b)** Thermo-magnetic analysis of the corresponding heat-treated CM powders and comparison with the bulk and HG4h600WQ powder.

As regards the post-annealed HEBM-8h powders, by applying the same annealing conditions, from the RT-XRD measurement of 8HEBM300WQ powder (**Fig. 8(a)**) it emerges a still highly disordered phase after annealing at 300°C, as previously observed for the 2CM300WQ powder. This fact highlights that the selected annealing temperature is not sufficient to permit the required atomic mobility for the defects annihilation and atomic reordering processes, which agrees to what reported by Tian *et al.* [29] about the beginning of the reordering process on heating above 360°C.

With the subsequent increase of annealing temperature to 400°C-500°C, it is observed an increase of crystallinity and the gradual recovery of the cubic austenitic phase, which presents the magnetic Curie transition at around 360 K (**Fig. 8(b)**), thus close to what expected and revealed also for the 2CM500WQ powder (**Fig. 7(b)**). However, at room-temperature, no traces of the martensitic phase can be detected by XRD analysis.

On further increasing the annealing temperature to 790°C, a partial recovery of the martensite phase can be observed for the 8HEBM790WQ powder, as denoted by the appearance of some (yet few and broad) characteristic reflections of the 7M, similarly to what detected for the 2CM500WQ sample. The corresponding magnetic susceptibility measurement (**Fig. 8(b)**), however, reveals that the martensitic transformation behaviour is still weak, and the structural transition appears to be decoupled from the magnetic one and shifted to lower temperatures. Therefore, it turns out that to fully recover the original martensitic phase transition an annealing at temperatures above 790°C is required, in accord to Tian *et al*. [31] for Ni-Mn-Ga particles prepared by vibration ball-milling. Finally, by selecting the high annealing temperature of 1000°C, even for the 8HEBM1000WQ particles the RT-XRD pattern shows a gradual suppression of the modulated martensitic structure, with predominance of the peaks of the NM phase (**Fig. 8(a)**). Moreover, the magneto-structural transition of this powder is significantly broad and shifted to higher temperatures (**Fig. 8(b)**).

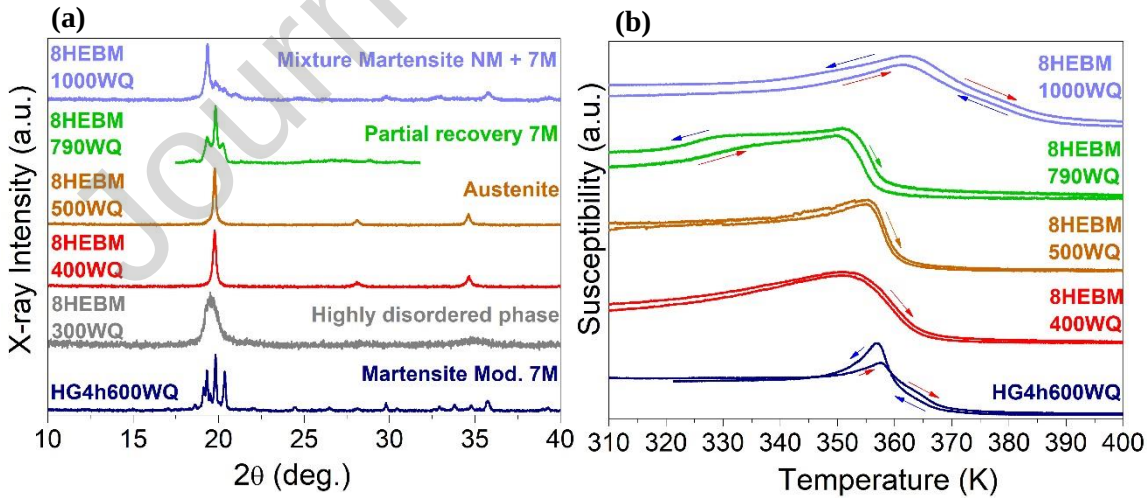

Figure 8: **(a)** Room-temperature XRD analysis of the post-annealed HEBM-8h powders of $Ni_{49.4}Mn_{30.3}Ga_{20.3}$ by varying the annealing temperatures, and comparison with the post-annealed hand-grinded powders (HG4h600WQ). **(b)** Study of the corresponding temperature-dependent magnetic susceptibility measurements.

The M(T) measurements in high field ($\mu_0 H$ = 1 T) of **Fig. 9**, instead, show that for the properly annealed powder batches there is a general enhancement of the saturation magnetization of the martensite with respect to the bulk.

At the fixed temperature of 100 K, the magnetization increases by 19.89% and 24.96% of that of the bulk for the 2hCM4h500SC and the HG4h600WQ powders, respectively. Moreover, for the CM-2h powder it is observed that the annealing at 500°C, for 4 h, followed by slow cooling, leads to a higher saturation magnetization as compared to the annealing treatment for 1-4 h, at 630°C, followed by water quenching. On the contrary, for the HG powder, the annealing temperature of 600°C and the water quenching are better conditions for increasing the net magnetization change across the transition, as compared to the annealing at 500°C followed by slow cooling.

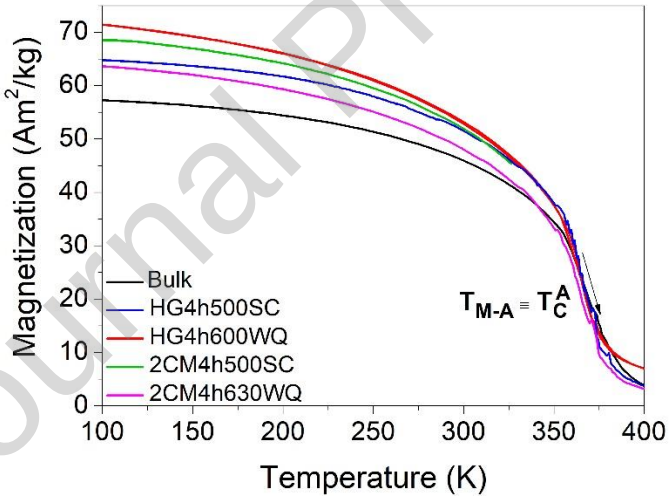

Figure 9: Temperature-dependent magnetization curves, at applied magnetic field of 1 T, for the $Ni_{49.4}Mn_{30.3}Ga_{20.3}$ bulk and post-annealed powders samples.

The above-presented results point out that both the HG and CM-2h powders can recover a well-defined 7M modulated martensite and a sharp coupled magneto-structural transformation after optimized annealing treatments. The best annealing conditions are a temperature of 500°C-630°C, an annealing time of 4 h, and a slow-cooling rate, for the cryo-milled particles. Instead, for the 8 h-milled particles with the

high-energy vibration ball-mill, the recovery of the martensitic phase at around room temperature requires an annealing temperature ≥ 800°C and the careful tuning of annealing time (≥ 4 h).

Apart from these differences, an excessively high annealing temperature of 1000°C has the common effect, in both types of CM-2h and HEBM-8h powders, of destabilizing the 7M modulated phase of the martensite, leading to the appearance of the NM martensitic structure and the change of the susceptibility behaviour closer to the as-grinded powder one.

3.5. Post-annealed Ni-Mn-Cu-Ga powders

Based on the above-illustrated results for Ni-Mn-Ga powders, the HG and CM powders of Ni-Mn-Cu-Ga were annealed at 500°C and 630°C for 4 h (**Table 2**).

From the comparison of the high-field M(T) curves in **Fig. 10(a)**, it is noticed that all the annealed powders retrieve the single magneto-structural transformation, which is less sharp, shifted to lower temperatures, and accompanied by a smaller thermal hysteresis (5-6 K) as compared to the bulk.

For the HG and CM powders, first it emerges that the annealing temperature of 500°C, combined with a rapid cooling rate (water quenching), leads to a significant shift to lower temperatures of the transformation, closer to room-temperature, and to a reduction of the saturation magnetization as compared to the annealing at 630°C. Indeed, the HG4h630WQ and 2CM4h630SC powders show a better recovery of the magneto-structural transition, and, after the slow cooling rate, a further rightward shift of the transition temperatures. Secondly, it is noted that, upon the same annealing conditions, for the ball-milled particles the transformation broadening is more pronounced than the HG ones and it deteriorates as a function of the milling duration, as

visible for the 3CM4h630WQ powder. Thirdly, it is observed that with respect to the bulk, apart from the lower transformation sharpness, there is no evident trace of secondary phases and a lower magnetic signal is retained at 340 K. Finally, the highest saturation magnetization for the annealed powders is lowered by only 6.5% than that of the bulk.

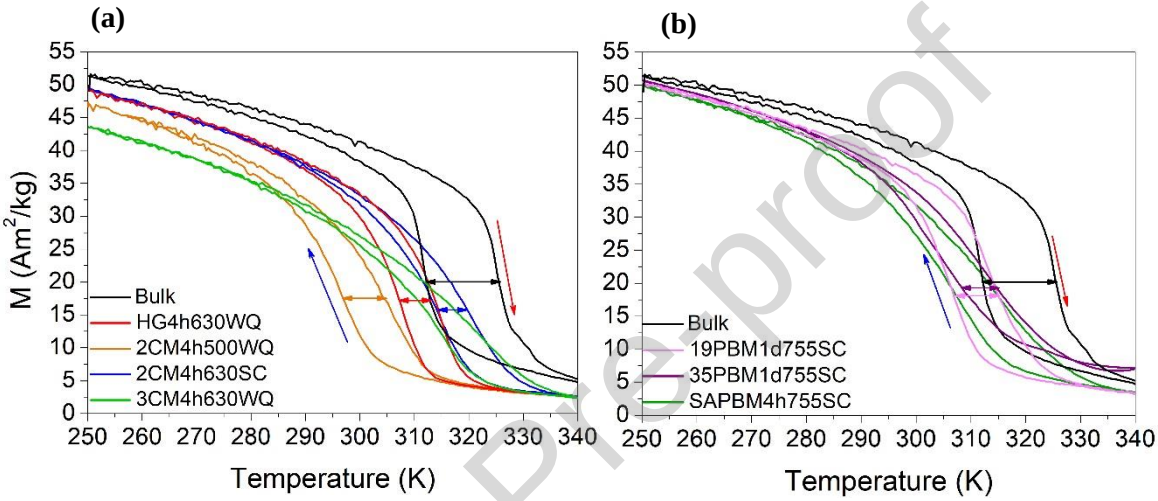

Figure 10: M-T curves at applied magnetic field of 1T for $Ni_{49.7}Mn_{18.7}Cu_{6.4}Ga_{25.2}$ **(a)** bulk, post-annealed hand-grinded, post-annealed cryo-milled powders and **(b)** post-annealed powders planetary ball-milled with isopropanol or with surfactant-assistance.

For the PBM powders processed for several hours with isopropanol, it was performed an annealing treatment at 755°C for one day, followed by slow cooling rate (19PBM1d755SC and 35PBM1d755SC samples). Instead, for the powders prepared in a two-steps process, of CM for 3 h and SAPBM for 14 h, it was applied the same annealing temperature, 755°C, but for a shorter annealing time of 4 h, followed by slow cooling as well (SAPBM4h755SC, **Table 2**).

The effect of the thermal treatments on the recovery of the original coupled magneto-structural phase transition is shown in **Fig. 10(b)**, where the M(T) measurements of the powders are compared to the bulk one.

It is interesting to notice that the transformation is retrieved at nearly the same temperature for the three batches of post-annealed PBM powders, accompanied by a similar thermal hysteresis and saturation magnetization of the martensite. These features are decreased with respect to the bulk, similarly to what before described for the post-annealed CM powders (**Fig. 10(a)**), but the 19PBM1d755SC sample shows a significant improvement in transformation sharpness. By contrast, for the 35PBM1d755SC powder, it is recognized an increase of both transformation broadening and magnetic moment at high temperature, thus denoting the presence of phase inhomogeneity.

By XRD measurements as a function of temperature, the structural martensitic transformation of the different annealed powders has been detected and the martensitic phase has been identified with a monoclinic-distorted 7M modulated superstructure.

For instance, in **Fig. 11**, it is displayed the change of the XRD pattern on decreasing the temperature from 350 K (only cubic austenitic phase) down to 20 K (only 7M modulated martensite) for the HG4h630WQ powder. The lattice parameters of the two phases are listed in **Table 4**. It is noticed that at 305 K the martensitic reflections are mixed with the residual traces of the cubic austenite, since the martensitic transformation finishes in cooling only at around 300 K, as visible from **Fig. 10(a)**. At 20 K, instead, it is possible to detect the shift to higher angles of some 7M martensitic peaks, due to the thermal lattice contraction.

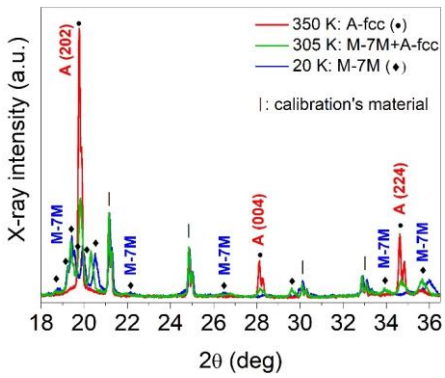

Figure 11: XRD spectra at three temperatures 350-305-20 K for the annealed HG4h630WQ powder of $Ni_{49.7}Mn_{18.7}Cu_{6.4}Ga_{25.2}$ compound.

The SEM analysis has pointed out that the post-annealed powders have maintained an elongated and thin shape, avoiding agglomeration and/or sintering even after long annealing treatments at high temperature. Rather, the latter have led to recrystallization and grain-growth phenomena, as visible in the SEM image of **Fig. 12(b)** for the 35PBM1d755SC powder, from which it is also possible to visualize the propagation of the martensitic twin lamellae within and across the grains.

Furthermore, by means of sonication and subsequent centrifugation of the SAPBM4h755SC powder batch, the bigger micrometric particles were separated from the supernatant ones, which have shown a particle length ranging from 700 to 250 nm and a thickness of 100-200 nm (see for instance **Fig. 12(a)**).

Therefore, the conducted investigation on the annealing treatments for Ni-Mn-Cu-Ga particles has brought about the assessment of the recovery of the coupled magneto-structural transformation by tuning both the annealing temperature, between 630-755°C, and the annealing time, from 4 h to 24 h, on the base of the selected milling time. Moreover, it has been highlighted the possibility to obtain, also after the applied thermal treatment, a small quantity of sub-micron particles among the batch of post-annealed surfactant-assisted planetary ball-milled powder.

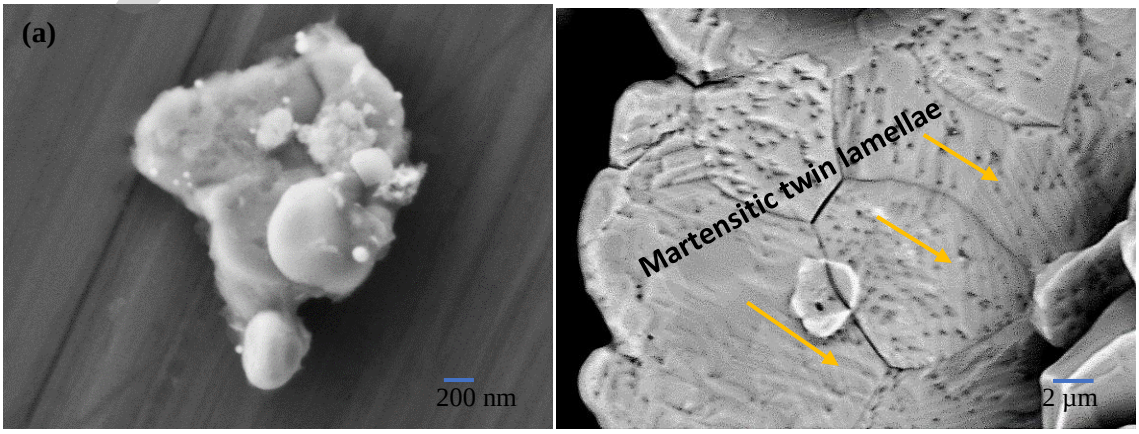

Figure 12: SEM images in SE and BSE of the $Ni_{49.7}Mn_{18.7}Cu_{6.4}Ga_{25.2}$ **(a)** 3CM14SAPBM4h755SC powder, showing the submicron size of the particle, and **(b)** 35wPBM24h755SC powder, highlighting the occurrence of recystallization and propagation of the martensitic twin lamellae.

4. Discussion

4.1. Effect of milling parameters

The results obtained for the as-milled particles have evidenced the strong impact of the selected milling parameters, as energy, time, and atmosphere, on particles' morphology, structure, and magnetic properties.

At the first, lower energetic level of crushing, i.e., for the HG particles, the martensitic phase is stabilized to higher temperatures, as shown for Ni-Mn-Ga in **Fig. 4**, or the transformation temperature range is increased with respect to the bulk, as displayed for Ni-Mn-Cu-Ga in **Fig. 6(b)**. These effects are compatible with the accumulation of elastic strain energy in the microstructure, in form of internal constraints and energy barriers, to be overcome with the thermal supply [36,38]. Furthermore, it is supposed that the spreading of the transition over a larger temperature interval could also depend on the separation into small, non-interacting particles, leading to a more random distribution of transformation temperature as compared to a single bulk fragment [24].

In addition, it has been observed a reduction of the saturation magnetization of the martensite, which can be ascribed to the increase of the surface-to-volume ratio and the defects concentration, due to the strong sensitivity of the magnetic interactions to the changes in the interatomic distances and Mn atoms surroundings [36,39,40].

For the Ni-Mn-Ga ball-milled powder, the increase of milling energy by increasing the milling time, during both cryogenic and room temperature ball-milling processes, leads to the structural transformation from the tetragonal martensitic phase to a disordered cubic phase. This effect is caused by the atomic disorder and the large lattice distortions induced by the repeated energetic collisions between powder and grinding media [39–41]. Among the two methods employed, the HEBM process appears to be more energetic than the CM one, since it leads faster to the structural change to the

disordered fcc phase (**Fig. 3(b)**). Nevertheless, this transformation is only delayed to a higher milling energy (by increasing the shaking frequency) or longer milling time (from 1 to 2 h), rather than being inhibited during the milling at cryogenic temperatures (**Fig. 3(a)**).

Instead, significant differences in particle morphology and size distribution have been recognized between the CM and HEBM particles. The change in morphology can be connected to the dependence on the environmental temperature (global and local) of the plastic deformation process and stress-recovery of the system. In fact, at cryogenic temperatures the material subjected to the mechanically induced stresses is cooled down and remains in the distorted anisotropic shape created by the martensitic variant reorientation during the stresses applied by ball-milling. Whereas, without coolant during the dry HEBM process, the rapid increase of temperature, which can locally exceed 1000°C under gaseous atmosphere [42], leads the particles to recover their original shape prior to the mechanical deformation and/or to transform to the more isotropic cubic structure, due to the atomic disorder [41]. Interestingly, for those particles it has been observed a partial recovery of the austenitic phase by increasing the milling time (**Fig. 3(b)**), which suggests that the local temperature and pressure can be significantly enhanced, thus promoting the rearrangement of dislocations and the annihilation of lattice defects [43]. Accordingly, such phenomenon gives rise to an inhomogeneous batch of powder, where the particles have different degrees of recovery of shape and atomic order.

On the other hand, the different size distribution between the CM and HEBM particles is ascribable to the number and dimensions of the balls used (see sect. **2.2.**).

As highlighted by the minimum particle length achievable, even after increasing the milling time to 8 h (see **Fig. 2(b)**), it follows that the HEBM method has a lower effect on particle size reduction, especially on particle thickness (10 μm), with respect to 2 h

of CM process (2-5 μm). However, this result appears to be in contrast with what reported by Wang *et al*. [32] about the possibility to achieve Ni_2MnGa nanoparticles after 8 h of high-energy ball-milling with SPEX-8000 laboratory mill, which is the same route here replicated. This contradiction can be overcome by supposing that the authors claim that the achieved coherent crystallites are at the nanoscale but not the particles themselves. Otherwise, some crucial experimental details on particles' preparation could have been missed or not clearly underlined in Refs. [32,44].

The suppression of the magnetic susceptibility signal after both types of ball-milling process (**Fig. 4**) has to be inferred, instead, to the accumulation of anti-phase boundaries, dislocations and structural defects, which induce internal and superficial atomic disorder thus altering the interatomic distances, site occupation and surroundings of the Mn atoms [39,40]. In turn, these phenomena affect and change the sign and amplitude of the magnetic exchange interactions, from ferromagnetic to antiferromagnetic, thus reducing the total magnetic moment to zero [39,40,45].

Differently from the Ni-Mn-Ga particles, the Ni-Mn-Cu-Ga CM ones have not shown the structural transformation to the cubic phase, even by increasing the milling time to 3 h, and, interestingly, they have not revealed, from the structural point of view, any significant dependence on the milling atmosphere, time, and type of ball-mill (**Fig. 6(a)**).

These features are ascribable to the peculiar mechanical behaviour of the Ni-Mn-Cu-Ga system under compressive strengths, which appears to be more ductile as compared to the Ni-Mn-Ga ternary compound [46,47].

Furthermore, it has been recently shown that Ni-Mn-Cu-Ga bulk polycrystalline samples are able to easily switch the crystallographic orientation of the martensitic variants under low applied stress, leading to a texturing of the compound [13]. This is

also expected to be characteristic of the crushed/milled powders of the same composition, and it could be responsible of both the anisotropic lattice strain observed from the XRD measurements and the elongation tendency highlighted in the SEM analysis.

Reasonably, the onset of texturing enables a higher lattice compatibility between neighbouring grains, which, together with an enhanced ductility, can account for the better mechanical resistance and phase stability against the induced lattice deformations and defects in the Ni-Mn-Cu-Ga ball-milled particles as compared to the Ni-Mn-Ga ones.

The decrease of the thermal hysteresis observed in the fine HG powder of Ni-Mn-Cu-Ga (**Fig. 6(b)**) deserves a particular attention. In fact, such a reduction of the energy dissipation during the formation of the martensite is an unusual phenomenon and must be investigated considering the role of particle/grain size in relation to the characteristic length scales of grain-boundary and phase-boundary.

As discussed by Li *et al*. [25] and Sun *et al*. [48], from both the theoretical and experimental point of view, the transition behaviour of nano-grained shape memory alloys differs significantly from that of coarse-grained counterparts, due to the gradual thickening and hence dominance of the interfaces over the bulk crystallite energy. This fact can bring about fundamental changes in thermal and mechanical responses of the material, such as the almost vanishing of the hysteresis losses and an ultrahigh strength.

On the other hand, also when the grain size is large enough to be comparable with the sample size, the hysteresis decreases [49]. In the present case, after only a soft hand-grinding in a mortar, the grain reduction to the nanoscale is unlikely, and, rather, it can be supposed that the obtained particles are single crystalline with a single variant twin structure, for the effect of variants' reorientation under applied compressive stress. This, in turn, enables a higher lattice coherency inside the particles, with a sensible reduction

of the frictional resistance from differently oriented twin boundaries to the phase front motion (lower thermal hysteresis) [36,50].

4.2. Effect of annealing treatment

The restoring of the magnetic and magneto-structural properties in milled powders of Ni-Mn-Ga and Ni-Mn-Cu-Ga was obtained by means of proper annealing treatments, which have a crucial role in modifying the atomic order and in increasing the phase homogeneity of the particles.

Concerning the hand-grinded powders of both Ni-Mn-Ga and Ni-Mn-Cu-Ga compounds, thermal treatment at 630°C restores the magneto-structural transition observed in the starting bulk samples. Moreover, the transition of the hand-grinded powders results to be smoother than the bulk. This fact highlights the possibility to release the mechanically induced stresses and concomitantly to reduce the concentration gradients by grinding the bulk sample and subsequently heating up, thus improving the phase homogenization and the functional properties of the compounds.

For the ball-milled powders, it has been observed that the pivotal role in the atomic reordering process is played by the annealing temperature, which has to be increased from 630°C to 800°C for Ni-Mn-Ga or to 755°C for Ni-Mn-Cu-Ga, depending on the milling energy and time adopted. Besides, also the cooling rate must be adjusted to avoid the shift to lower temperatures of the transition and the decrease of the saturation magnetization. Indeed, the water quenching prevents reaching the equilibrium atomic order allowed by the stoichiometry of the compound [51], with detrimental effects on the magnetic interactions and the thermodynamics of the martensitic transformation.
Further, the annealing time is an important parameter to permit the recrystallization process and the grain-growth phenomenon in particles milled for several hours, hence

containing a higher concentration of defects. The increase of annealing time can reduce the number of grain-boundaries and inhomogeneities, acting as microstructural energy barriers for the formation of the martensite, and, then, can enhance the lattice relaxation, till the formation of a more uniform and unconstrained microstructure.

In this respect, the less defined magnetic susceptibility curves exhibited by the post-annealed HEBM-8h powders of Ni-Mn-Ga (**Fig. 8(b)**), as compared to the CM-2h ones (**Fig. 7(b)**), are ascribable to an insufficient annealing time (1 h) for finalizing the ordering process and the stresses' release, hence for recovering the original sharp magneto-structural transformation.

Despite the optimization of the annealing conditions, an unavoidable increase of the transformation temperature range characterizes the magneto-structural behaviour of the ball-milled particles as compared to the coarser hand-grinded ones and the bulk.

This fact can be generally inferred to the lack of stress-coupling between the particles and, hence, to the random distribution of their transformation temperatures and crystallographic orientation [24]. However, as reported in [36,50,52], it also depends on the amount of stored elastic energy E_{el}, which increases in the smaller particles and requires an additional undercooling for the completion of the martensite transformation, thus decreasing the martensite finish temperature.

In **Fig. 10(b)**, the Ni-Mn-Cu-Ga 35PBM1d755SC and SAPBM4h755SC powders show a larger transformation broadening than the 19PBM1d755SC one, thus highlighting a higher accumulation of elastic strain energy. This can arise from internal stresses not-released or even created by the annealing treatment, which influence and change the accommodation and dissipation of the elastic stresses generated by the martensitic transformation itself [38]. Nevertheless, the powders present a similar hysteresis width, which implies the same degree of energy dissipation by frictional work.

It is worth stressing that for all the post-annealed powders of Ni-Mn-Cu-Ga the thermal hysteresis decreases with respect to the original bulk. This fact points out the occurrence of a lower frictional resistance to the phase boundaries movement or more compatible lattice relations at the interacting interfaces, associable with higher coherency strains between the transformable volume regions [50]. The reason for that could be the existence of a different transformation path from austenite to martensite between bulk and microparticles [49]. This would require, out of the scope of this work, a detailed crystallographic investigation of the martensite structure as a function of the sample dimension.

Nevertheless, it can be supposed that first the texturing by application of mechanical stresses and secondly the microstructural recovery during the heat treatment, through annihilation of the initial defects and/or recrystallization process, have beneficial effects in the overall reduction of the hysteresis losses for the microparticles [13,36]. It is also worth considering that the characteristic elongated and flat morphology of the particles, where large equiaxed grains span the whole particle cross-section (**Figs. 12(a)-(b)**), could have offered favourable geometrical conditions for the propagation of the twin-related martensitic variants with extremely low twinning stress [22,53].

Finally, it has been observed that an annealing treatment at very high temperatures (1000°C) induces in the CM and HEBM powders of Ni-Mn-Ga an irreversible change of the martensitic structure, from the 7M modulated to the tetragonal NM phase (**Figs. 7(a)-8(a)**). Moreover, it has been noticed that the thermomagnetic behaviour of these annealed powders is almost identical to that of the HG powder (**Figs. 7(b)-8(b)**), such as the shift to a higher temperature of the overlapped magneto-structural transformation and the increase of broadening. Therefore, in analogy to the mechanically induced stresses, an excessively high thermal energy can apport significant variations in the

internal lattice strain, to which the martensitic phase is particularly sensitive for the peculiar ferro-elastic properties [3]. It derives that, after rapidly cooling from high temperature, in the austenitic phase, the accumulated stresses induce the inter-martensitic transformation from the 7M modulated to the tetragonal $L1_0$ phase. The latter, indeed, is the most stable structure against high thermal and mechanical stresses, as reported in [54,55]. The peculiar mechanism underlying this stress-induced transformation is theoretically and experimentally explained as a process of detwinning of the 7M modulated structure [54,55] and it is characteristic of many types of shape memory alloys [49,54–56].

Beyond this phenomenology, it is worth stressing that the selected high annealing temperature of 1000°C is well-above the expected transition temperature $T_t^{L2_1/B2}$=780°C [51] from the ordered $L2_1$ Heusler phase to the disordered $B2$ structure of the austenite. Thereby, concerning the change of the martensitic structure (or microstructure), it should be considered also a possible contribution of the thermally induced configurational disorder in the Heusler cell, to which the Mn-rich compositions are particularly sensitive [57]. Reasonably, the increase of atomic disorder can lead to both structural and magnetic instability, thus affecting the martensitic transformation and the martensite structure itself. It follows that both an increase of internal stresses and a reduction of the degree of atomic order have detrimental effects on the magneto-thermal properties of the Ni-Mn-Ga compound, independently on the particles' morphology, since equally observed for HG, CM, and HEBM powders.

5. Conclusions

This study has shown the effect of different milling methods on the reduction of particle size, from the macro to the micro and/or sub-micro-meter scale, of two Heusler compounds, $Ni_{49.4}Mn_{30.3}Ga_{20.3}$ and $Ni_{49.7}Mn_{18.7}Cu_{6.4}Ga_{25.2}$. It has been demonstrated, specifically for the latter compound, the effectiveness of combining the cryo-milling

method with the surfactant-assisted planetary ball-milling to obtain nanoparticles, even under a low rotational speed of 300 rpm, by carefully tuning the amount of surfactant (oleic acid 20 wt. %) and the milling time (8-14 h).

A systematic investigation of the morphology, crystal structure and magnetic properties of the as-milled particles has pointed out the detrimental effect of the details of the milling process (energy involved and milling atmosphere) on the functional properties of the material, even after few hours of milling. Particularly, this fact has been observed for Ni-Mn-Ga, whereas the Ni-Mn-Cu-Ga ball-milled powders have shown a higher structural stability and a higher anisotropic lattice strain against the mechanical deformation process, linkable to a more ductile mechanical behaviour and an easier switching of the martensitic variants.

Several post-milling annealing treatments have been studied to restore the original atomic order and the phase transitions. An optimal annealing treatment at 500-630°C, for 4 h, followed by a slow-cooling rate, enables the recovery for both the Ni-Mn-Ga and Ni-Mn-Cu-Ga microparticles prepared by hand-grinded and cryo-milling for 2 h. For the longer-time milled powders, as the Ni-Mn-Cu-Ga particles planetary ball-milled with isopropanol or surfactant-assistance and the Ni-Mn-Ga ones subjected to the high-energy vibration ball-milling, an increase of annealing temperature to 755°C and 800°C, respectively, together with an increase of annealing time to several hours (up to 24 h), are necessary requirements. Interestingly, these long-time and high-temperature heat treatments have induced the recrystallization and grain-growth phenomena, but without causing sintering and agglomeration, thus preserving the flaky morphology and sub-micro-meter size of the as-prepared particles.

With respect to the bulk behaviour, the annealed particles show significant improvements, such as the enhancement of phase homogeneity, reduction of thermal hysteresis, and increase of saturation magnetization (or only a slight decrease). By

contrast, the coupled magneto-structural transformation appears less sharp, and the transition temperatures are decreased. These differences have been ascribed to the microstructural variations brought about by the mechanical stresses, first, and the thermal treatment, secondly, as the separation into small non-interacting pieces, the different defects concentration and degree of atomic order, the reduction of compositional gradients, and the increase of grain-size over particle thickness ratio.

In conclusion, the demonstrated feasible optimization of both the preparation of sub-micron particles, by ball-milling methods, and the recovery of the coupled magneto-structural transformation, through annealing treatments, opens up new potential applications at the micro and nanoscale for the multifunctional Ni-Mn-Ga and Ni-Mn-Cu-Ga compounds, such as in energy-conversion technology, sensing/actuation, and/or biomedicine.

Acknowledgements

G. Cavazzini would like to acknowledge the Functional Material Group at TU-Darmstadt for their hospitality and cooperation. This work has been partially funded by Fondazione Cariparma (PhD scholarship of G. Cavazzini). O. Gutfleisch thanks Fondazione Cariparma for a three-year visiting professorship at the University of Parma, in the framework of the TeachInParma project.

6. References

[1] F. Albertini, M. Solzi, A. Paoluzi, L. Righi, Magnetocaloric properties and magnetic anisotropy by tailoring phase transitions in NiMnGa alloys, Mater. Sci. Forum. 583 (2008) 169–196. https://doi.org/10.4028/www.scientific.net/msf.583.169.

[2] P. Entel, V.D. Buchelnikov, V. V. Khovailo, A.T. Zayak, W.A. Adeagbo, M.E. Gruner, H.C. Herper, E.F. Wassermann, Modelling the phase diagram of magnetic shape memory Heusler alloys, J. Phys. D. Appl. Phys. 39 (2006) 865–889. https://doi.org/10.1088/0022-3727/39/5/S13.

[3] M. Kohl, M. Gueltig, V. Pinneker, R. Yin, F. Wendler, B. Krevet, Magnetic shape memory microactuators, Micromachines. 5 (2014) 1135–1160. https://doi.org/10.3390/mi5041135.

[4] V. Gschneidner, K. Pecharsky, Thirty years of near room temperature magnetic cooling: Where we are today and future prospects, Int. J. Refrig. 31 (2008).

[5] J. Liu, T. Gottschall, K.P. Skokov, J.D. Moore, O. Gutfleisch, Giant magnetocaloric effect driven by structural transitions, Nat. Mater. (2012). https://doi.org/10.1038/nmat3334.

[6] O. Gutfleisch, T. Gottschall, M. Fries, D. Benke, I. Radulov, K.P. Skokov, H. Wende, M. Gruner, M. Acet, P. Entel, M. Farle, Mastering hysteresis in magnetocaloric materials, Philos. Trans. R. Soc. A Math. Phys. Eng. Sci. 374 (2016). https://doi.org/10.1098/rsta.2015.0308.

[7] O. Gutfleisch, M.A. Willard, E. Brück, C.H. Chen, S.G. Sankar, J.P. Liu, Magnetic materials and devices for the 21st century: Stronger, lighter, and more energy efficient, Adv. Mater. 23 (2011) 821–842. https://doi.org/10.1002/adma.201002180.

[8] Z. Li, Y. Zhang, C.F. Sánchez-Valdés, J.L. Sánchez Llamazares, C. Esling, X. Zhao, L. Zuo, Giant magnetocaloric effect in melt-spun Ni-Mn-Ga ribbons with magneto-multistructural transformation, Appl. Phys. Lett. (2014). https://doi.org/10.1063/1.4863273.

[9] Z.B. Li, J.L. Sánchez Llamazares, C.F. Sánchez-Valdés, Y.D. Zhang, C. Esling, X. Zhao, L. Zuo, Microstructure and magnetocaloric effect of melt-spun Ni 52Mn 26Ga 22 ribbon, Appl. Phys. Lett. (2012). https://doi.org/10.1063/1.4704780.

[10] D. Zhao, T. Castán, A. Planes, Z. Li, W. Sun, J. Liu, Enhanced caloric effect induced by magnetoelastic coupling in NiMnGaCu Heusler alloys: Experimental study and theoretical analysis, Phys. Rev. B. 96 (2017). https://doi.org/10.1103/PhysRevB.96.224105.

[11] T. Kanomata, K. Endo, N. Kudo, R.Y. Umetsu, H. Nishihara, M. Kataoka, M. Nagasako, R. Kainuma, K.R.A. Ziebeck, Magnetic moment of cu-modified Ni2MnGa magnetic shape memory alloys, Metals (Basel). 3 (2013) 114–122. https://doi.org/10.3390/met3010114.

[12] S. Stadler, M. Khan, J. Mitchell, N. Ali, A.M. Gomes, I. Dubenko, A.Y. Takeuchi, A.P. Guimarães, Magnetocaloric properties of Ni 2Mn 1-xCu xGa, Appl. Phys. Lett. (2006). https://doi.org/10.1063/1.2202751.

[13] M. V. McLeod, D. Bayer, Z. Turgut, A.K. Giri, B.S. Majumdar, Significant enhancement of magnetocaloric effect in a NiMnCuGa Heusler alloy through textural modification, J. Appl. Phys. (2020). https://doi.org/10.1063/5.0003366.

[14] A. Espinosa, J. Kolosnjaj-Tabi, A. Abou-Hassan, A. Plan Sangnier, A. Curcio, A.K.A. Silva, R. Di Corato, S. Neveu, T. Pellegrino, L.M. Liz-Marzán, C. Wilhelm, Magnetic (Hyper)Thermia or Photothermia? Progressive Comparison of Iron Oxide and Gold Nanoparticles Heating in Water, in Cells, and In Vivo, Adv. Funct. Mater. 28 (2018). https://doi.org/10.1002/adfm.201803660.

[15] R. Hergt, S. Dutz, R. Müller, M. Zeisberger, Magnetic particle hyperthermia: Nanoparticle magnetism and materials development for cancer therapy, J. Phys.

Condens. Matter. (2006). https://doi.org/10.1088/0953-8984/18/38/S26.

[16] M.P. Caputo, C. V. Solomon, A facile method for producing porous parts with complex geometries from ferromagnetic Ni-Mn-Ga shape memory alloys, Mater. Lett. (2017). https://doi.org/10.1016/j.matlet.2017.04.112.

[17] A. Mostafaei, K.A. Kimes, E.L. Stevens, J. Toman, Y.L. Krimer, K. Ullakko, M. Chmielus, Microstructural evolution and magnetic properties of binder jet additive manufactured Ni-Mn-Ga magnetic shape memory alloy foam, Acta Mater. (2017). https://doi.org/10.1016/j.actamat.2017.04.010.

[18] M. Takhsha Ghahfarokhi, F. Casoli, S. Fabbrici, L. Nasi, F. Celegato, R. Cabassi, G. Trevisi, G. Bertoni, D. Calestani, P. Tiberto, F. Albertini, Martensite-enabled magnetic flexibility: The effects of post-growth treatments in magnetic-shape-memory Heusler thin films, Acta Mater. (2020). https://doi.org/10.1016/j.actamat.2020.01.049.

[19] P. Ranzieri, S. Fabbrici, L. Nasi, L. Righi, F. Casoli, V.A. Chernenko, E. Villa, F. Albertini, Epitaxial Ni-Mn-Ga/MgO(1 0 0) thin films ranging in thickness from 10 to 100 nm, Acta Mater. (2013). https://doi.org/10.1016/j.actamat.2012.09.056.

[20] M. Campanini, L. Nasi, S. Fabbrici, F. Casoli, F. Celegato, G. Barrera, V. Chiesi, E. Bedogni, C. Magén, V. Grillo, G. Bertoni, L. Righi, P. Tiberto, F. Albertini, Magnetic Shape Memory Turns to Nano: Microstructure Controlled Actuation of Free-Standing Nanodisks, Small. (2018). https://doi.org/10.1002/smll.201803027.

[21] M.F. Qian, X.X. Zhang, L.S. Wei, L. Geng, H.X. Peng, Structural, Magnetic and Mechanical Properties of Oligocrystalline Ni-Mn-Ga Shape Memory Microwires, Mater. Today Proc. (2015). https://doi.org/10.1016/j.matpr.2015.07.351.

[22] D.C. Dunand, P. Müllner, Size effects on magnetic actuation in Ni-Mn-Ga shape-memory alloys, Adv. Mater. 23 (2011) 216–232. https://doi.org/10.1002/adma.201002753.

[23] J. Liu, N. Scheerbaum, S. Kauffmann-Weiss, O. Gutfleisch, NiMn-based alloys and composites for magnetically controlled dampers and actuators, Adv. Eng. Mater. (2012). https://doi.org/10.1002/adem.201200038.

[24] T. Gottschall, D. Benke, M. Fries, A. Taubel, I.A. Radulov, K.P. Skokov, O. Gutfleisch, A Matter of Size and Stress: Understanding the First-Order Transition in Materials for Solid-State Refrigeration, Adv. Funct. Mater. (2017). https://doi.org/10.1002/adfm.201606735.

[25] M.P. Li, Q.P. Sun, Nanoscale phase transition behavior of shape memory alloys — closed form solution of 1D effective modelling, J. Mech. Phys. Solids. (2018). https://doi.org/10.1016/j.jmps.2017.09.008.

[26] M. Broseghini, L. Gelisio, M. D'Incau, C.L. Azanza Ricardo, N.M. Pugno, P. Scardi, Modeling of the planetary ball-milling process: The case study of ceramic powders, J. Eur. Ceram. Soc. 36 (2016) 2205–2212. https://doi.org/10.1016/j.jeurceramsoc.2015.09.032.

[27] C. Suryanarayana, Mechanical alloying and milling, CRC Press, 2004. https://doi.org/10.4150/kpmi.2006.13.5.371.

[28] F. Zhou, S.R. Nutt, C.C. Bampton, E.J. Lavernia, Nanostructure in an Al-Mg-Sc Alloy Processed by Low-Energy Ball Milling at Cryogenic Temperature, Metall.

Mater. Trans. A. 34 A (2003).

[29] B. Tian, F. Chen, Y. Liu, Y.F. Zheng, Structural transition and atomic ordering of Ni49.8Mn28.5Ga21.7 ferromagnetic shape memory alloy powders prepared by ball milling, Mater. Lett. (2008). https://doi.org/10.1016/j.matlet.2008.01.071.

[30] B. Tian, F. Chen, Y.X. Tong, L. Li, Y.F. Zheng, Phase transformation and magnetic property of Ni-Mn-Ga powders prepared by dry ball milling, J. Mater. Eng. Perform. (2012). https://doi.org/10.1007/s11665-012-0365-2.

[31] B. Tian, F. Chen, Y.X. Tong, L. Li, Y.F. Zheng, Y. Liu, Q.Z. Li, Phase transition of Ni-Mn-Ga alloy powders prepared by vibration ball milling, J. Alloys Compd. (2011). https://doi.org/10.1016/j.jallcom.2011.01.104.

[32] Y.D. Wang, Y. Ren, Z.H. Nie, D.M. Liu, L. Zuo, H. Choo, H. Li, P.K. Liaw, J.Q. Yan, R.J. McQueeney, J.W. Richardson, A. Huq, Structural transition of ferromagnetic Ni2MnGa nanoparticles, J. Appl. Phys. (2007). https://doi.org/10.1063/1.2713370.

[33] D.B. Witkin, E.J. Lavernia, Synthesis and mechanical behavior of nanostructured materials via cryomilling, Prog. Mater. Sci. 51 (2006).

[34] V. Petrícek, M. Dušek, L. Palatinus, Crystallographic computing system JANA2006: General features, Zeitschrift Fur Krist. (2014). https://doi.org/10.1515/zkri-2014-1737.

[35] F. Albertini, L. Morellon, P.A. Algarabel, M.R. Ibarra, L. Pareti, Z. Arnold, E. Al., Magnetoelastic effects and magnetic anisotropy in Ni2MnGa polycrystals, J. Appl. Phys. 89 (2001).

[36] M. Qian, X. Zhang, Z. Jia, X. Wan, L. Geng, Enhanced magnetic refrigeration capacity in Ni-Mn-Ga micro-particles, Mater. Des. (2018). https://doi.org/10.1016/j.matdes.2018.03.062.

[37] A. Cakir, L. Righi, F. Albertini, M. Acet, M. Farle, S. Akturk, Extended investigation of intermartensitic transitions in Ni-Mn-Ga magnetic shape memory alloys: A detailed phase diagram determination, J. Appl. Phys. 114 (2013).

[38] Y. Chen, C.A. Schuh, Size effects in shape memory alloy microwires, Acta Mater. (2011). https://doi.org/10.1016/j.actamat.2010.09.057.

[39] F. Cugini, L. Righi, L. van Eijck, E. Brück, M. Solzi, Cold working consequence on the magnetocaloric effect of Ni50Mn34In16 Heusler alloy, J. Alloys Compd. (2018). https://doi.org/10.1016/j.jallcom.2018.03.293.

[40] B. Tian, F. Chen, Y. Liu, Y.F. Zheng, Effect of ball milling and post-annealing on magnetic properties of Ni49.8Mn28.5Ga21.7 alloy powders, Intermetallics. (2008). https://doi.org/10.1016/j.intermet.2008.08.002.

[41] C. Wen, A. Nouri, Surfactants in Mechanical Alloying/Milling: A Catch-22 Situation, Crit. Rev. Solid State Mater. Sci. 39 (2014).

[42] C. Dhand, N. Dwivedi, X.J. Loh, A.N. Jie Ying, N.K. Verma, R.W. Beuerman, R. Lakshminarayanan, S. Ramakrishna, Methods and strategies for the synthesis of diverse nanoparticles and their applications: A comprehensive overview, RSC Adv. (2015). https://doi.org/10.1039/c5ra19388e.

[43] S.M. Almotairy, A.F. Boostani, M. Hassani, D. Wei, Z.Y. Jiang, Effect of hot isostatic pressing on the mechanical properties of aluminium metal matrix

nanocomposites produced by dual speed ball milling, J. Mater. Res. Technol. (2020). https://doi.org/10.1016/j.jmrt.2019.11.043.

[44] D.M. Liu, Z.H. Nie, Y.D. Wang, Y.D. Liu, G. Wang, Y. Ren, L. Zuo, New sequences of phase transition in Ni-Mn-Ga ferromagnetic shape memory nanoparticles, Metall. Mater. Trans. A Phys. Metall. Mater. Sci. (2008). https://doi.org/10.1007/s11661-007-9435-8.

[45] D. Wu, S. Xue, J. Frenzel, G. Eggeler, Q. Zhai, H. Zheng, Atomic ordering effect in Ni 50Mn 37Sn 13 magnetocaloric ribbons, Mater. Sci. Eng. A. (2012). https://doi.org/10.1016/j.msea.2011.12.009.

[46] Y. Xin, Y. Li, Microstructure, mechanical and shape memory properties of polycrystalline Ni-Mn-Ga High temperature shape memory alloys, Mater. Sci. Eng. A. (2016). https://doi.org/10.1016/j.msea.2015.09.123.

[47] J. Wang, H. Wang, C. Jiang, Microstructure and mechanical properties of a Ni30Cu20Mn41.5Ga8.5 dual-phase shape memory alloy, Mater. Sci. Eng. A. (2013). https://doi.org/10.1016/j.msea.2013.04.111.

[48] Q. Sun, A. Aslan, M. Li, M. Chen, Effects of grain size on phase transition behavior of nanocrystalline shape memory alloys, Sci. China Technol. Sci. (2014). https://doi.org/10.1007/s11431-014-5505-5.

[49] N. Ozdemir, I. Karaman, N.A. Mara, Y.I. Chumlyakov, H.E. Karaca, Size effects in the superelastic response of Ni 54Fe 19Ga 27 shape memory alloy pillars with a two stage martensitic transformation, Acta Mater. (2012). https://doi.org/10.1016/j.actamat.2012.06.035.

[50] R.F. Hamilton, H. Sehitoglu, Y. Chumlyakov, H.J. Maier, Stress dependence of the hysteresis in single crystal NiTi alloys, Acta Mater. (2004). https://doi.org/10.1016/j.actamat.2004.03.038.

[51] V. Sánchez-Alarcos, V. Recarte, J.I. Pérez-Landazábal, G.J. Cuello, Correlation between atomic order and the characteristics of the structural and magnetic transformations in Ni-Mn-Ga shape memory alloys, Acta Mater. (2007). https://doi.org/10.1016/j.actamat.2007.03.001.

[52] N.M. Bruno, Y.J. Huang, C.L. Dennis, J.G. Li, R.D. Shull, J.H. Ross, Y.I. Chumlyakov, I. Karaman, Effect of grain constraint on the field requirements for magnetocaloric effect in Ni45Co5Mn40Sn10 melt-spun ribbons, J. Appl. Phys. (2016). https://doi.org/10.1063/1.4960353.

[53] R. Chulist, L. Straka, H. Seiner, A. Sozinov, N. Schell, T. Tokarski, Branching of {110) twin boundaries in five-layered Ni-Mn-Ga bent single crystals, Mater. Des. (2019). https://doi.org/10.1016/j.matdes.2019.107703.

[54] Y. Ge, N. Zárubová, O. Heczko, S.P. Hannula, Stress-induced transition from modulated 14M to non-modulated martensite in Ni-Mn-Ga alloy, Acta Mater. (2015). https://doi.org/10.1016/j.actamat.2015.02.028.

[55] Y. Liu, I. Karaman, H. Wang, X. Zhang, Two types of martensitic phase transformations in magnetic shape memory alloys by in-situ nanoindentation studies, Adv. Mater. (2014). https://doi.org/10.1002/adma.201400217.

[56] R.F. Hamilton, H. Sehitoglu, C. Efstathiou, H.J. Maier, Inter-martensitic transitions in Ni-Fe-Ga single crystals, Acta Mater. (2007). https://doi.org/10.1016/j.actamat.2007.05.003.

[57] V. V. Sokolovskiy, M.E. Gruner, P. Entel, M. Acet, A. Cakir, D.R. Baigutlin, V.D. Buchelnikov, Segregation tendency of Heusler alloys, Phys. Rev. Mat. 3 (2019).

Graphical Abstract

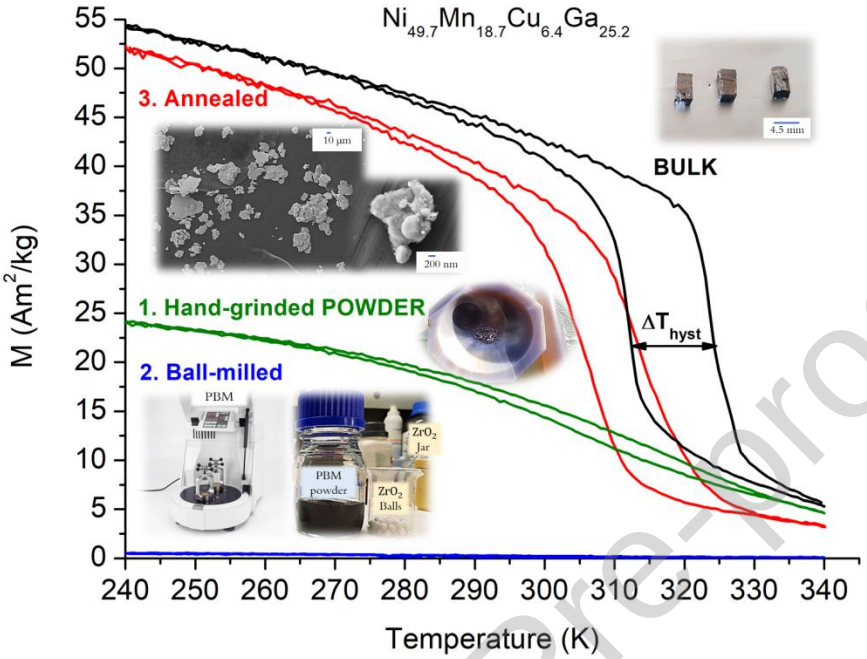

Credit Authors Statement

Greta Cavazzini: Investigation; Visualization; Conceptualization; Formal Analysis; Writing - Original draft preparation, Reviewing and Editing; Funding acquisition.

Francesco Cugini: Conceptualization; Validation; Reviewing.

Davide Delmonte: Resources.

Giovanna Trevisi: Resources.

Lucia Nasi: Resources.

Semih Ener: Validation; Reviewing.

David Koch: Resources.

Lara Righi: Resources; Reviewing.

Massimo Solzi: Supervision; Validation; Project administration; Reviewing.

Oliver Gutfleisch: Supervision; Project administration; Reviewing.

Franca Albertini: Supervision; Validation; Project administration; Reviewing.

Declaration of interests

☒ The authors declare that they have no known competing financial interests or personal relationships that could have appeared to influence the work reported in this paper.

☐The authors declare the following financial interests/personal relationships which may be considered as potential competing interests:

Highlights

- Micro and sub-micro-meter sized particles of Heusler compounds prepared by the top-down ball-milling technique
- Recovery of the initial bulk phase transitions through optimization of the annealing treatments depending on the milling conditions selected
- Tunability and improvement with respect to the bulk of the magneto-structural properties
- Avoidance of sintering and/or agglomeration between particles even during long annealing treatments at high temperature
- Higher phase stability and grain coherency during severe plastic deformation for Ni-Mn-Cu-Ga compound as compared to the ternary Ni-Mn-Ga one